Available online at www.sciencedirect.com

ScienceDirect

Geochimica et Cosmochimica Acta 281 (2020) 91–101

Geochimica et Cosmochimica Acta

www.elsevier.com/locate/gca

Seawater versus mantle sources of mercury in sulfide-rich seafloor hydrothermal systems, Southwest Indian Ridge

Chuanwei Zhu [a,b], Chunhui Tao [a,*], Runsheng Yin [b], Shili Liao [a], Weifang Yang [a], Jia Liu [a], Fernando J.A.S. Barriga [c]

[a] Key Laboratory of Submarine Geosciences, Second Institute of Oceanography, MNR, Hangzhou 310012, China
[b] State Key Laboratory of Ore Deposit Geochemistry, Institute of Geochemistry, Chinese Academy of Sciences, Guiyang 550081, China
[c] Departamento de Geologia, Faculdade de Ciências, Universidade de Lisboa, Lisboa, Portugal

Received 8 October 2019; accepted in revised form 6 May 2020; available online 15 May 2020

Abstract

The Southwest Indian Ridge (SWIR) is an ultraslow-spreading ridge where large hydrothermal fields (HFs) are widely distributed. The HFs differ in geological settings, basement rock compositions and mineral associations, but are commonly associated with massive sulfides and sulfide-rich hydrothermal vents that are rich in mercury (Hg). However, the source of Hg remains not well understood. This is a first report on the concentration and isotopic composition of Hg in sulfides from two large HFs, named Duanqiao and Yuhuang, in the SWIR. Sulfides from Duanqiao and Yuhuang showed elevated Hg concentrations, ranging from 3.5×10^2 to 8.1×10^3 ng/g and 4.4×10^2 to 4.4×10^4 ng/g, respectively, which suggest that seafloor mass sulfide deposits can be an important sink of Hg to the deep marine environment. In both HFs, pyrite (4.4×10^2–4.4×10^4 ng/g) and sphalerite (8.3×10^2–6.0×10^3 ng/g) show higher Hg concentrations than chalcopyrite (3.5×10^2 ng/g), suggesting that the replacement of Fe(II) and Zn(II) by Hg(II) is a major form of Hg incorporation in sulfides. Sulfides from Yuhuang show relatively larger δ^{202}Hg and Δ^{199}Hg ranges of −1.23 to −0.05‰ and −0.10 to 0.20‰, respectively, compared with those from Duanqiao (δ^{202}Hg: −0.63 to −0.12‰; Δ^{199}Hg: 0.02–0.10‰), suggesting that the Hg sources are different in the two HFs. The differences in Δ^{199}Hg suggest the dominance of magmatic/mantle Hg in the Duanqiao HF, but a mixture of magmatic/mantle and seawater Hg to the Yuhuang HF. We thus propose Hg isotopes as a potential source tracer of Hg in HFs and infer that magmatism may not only serve as a direct Hg source in HFs, but may also drive seawater circulation and cause the precipitation of Hg from hydrothermally circulated seawater.

Keywords: Mercury isotopes; Sulfides; Hydrothermal fields; southwest Indian ridge

1. INTRODUCTION

Mercury (Hg) is a globally distributed and redox-sensitive trace metal occurring in high concentrations in many terrestrial and marine environments (Selin, 2009; Gworek et al., 2016; Kim et al., 2016). The atmosphere and oceans play critical roles in the geochemical cycling of Hg (Selin, 2009). It is released to the environment through both natural sources (e.g., volcanoes, hydrothermal emission and biomass burning) and anthropogenic activities (e.g., fossil fuel combustion, nonferrous metal mining) (Pirrone et al., 2010). Mercury can undergo global transport in the atmosphere before it is removed from the atmosphere through wet and dry deposition processes (Amos et al., 2014). Once deposited to the oceans, a minor fractionation of mercury can be converted into methylmercury (MeHg), a neurotoxin that can accumulate along

* Corresponding author.
E-mail address: taochunhuimail@163.com (C. Tao).

https://doi.org/10.1016/j.gca.2020.05.008
0016-7037/

aquatic food chains, whereas the remainder continues to cycle through the land-atmosphere-ocean system for centuries to millennia before being sequestered in soils and sediments (Selin, 2009).

Mercury isotope geochemistry has been developed as a new tracer to understand the geochemical fate of Hg (Blum et al., 2014 and references therein). Mercury's naturally occurring stable isotopes (^{196}Hg, ^{198}Hg, ^{199}Hg, ^{200}Hg, ^{201}Hg, ^{202}Hg and ^{204}Hg) undergo both mass-dependent fractionation (MDF, usually defined as δ^{202}Hg) and mass-independent fractionation (MIF, usually defined as Δ^{199}Hg). Hg-MDF is omnipresent and occurs during almost all biological, abiotic chemical and physical activities, whereas Hg-MIF signals in natural samples are mainly related to photochemical processes (e.g., aqueous Hg (II) photoreduction and methylmercury degradation) (Bergquist and Blum, 2009; Blum et al., 2014). A large variation in Hg isotopic composition, ~8‰ for both δ^{202}Hg and Δ^{199}Hg, has been reported in different environmental pools (reviewed by Blum et al., 2014). More and more evidences indicate that hydrothermal processes can cause significant Hg-MDF, but cannot result in large Hg-MIF (Smith et al., 2005, 2008; Sonke et al., 2010; Yin et al., 2013, 2016a, 2019; Tang et al., 2017; Xu et al., 2018). Hg-MIF signals are therefore particularly useful in distinguishing the origin of Hg (e.g., syngenetic vs epigenetic) in hydrothermal systems, because Hg derived from magmatic/mantle materials is characterized by the absence of Hg-MIF (Δ^{199}Hg = ~0‰), whereas Hg sourced from soil/sediments, water/snow, atmospheric Hg species and biota samples showed significant Hg-MIF signals (Yin et al., 2016a and references therein).

Sources of Hg to the ocean include continental runoff, direct atmospheric deposition and hydrothermal vents (Mason et al., 2012). Globally, continental runoff and atmospheric deposition contribute with equal roles in mercury inputs to the ocean, but their contribution varies between coastal/shelf and open marine regions (Sunderland and Mason, 2007; Amos et al., 2014; Zhang et al., 2015). The isotopic signatures of Hg in continental runoff and atmospheric deposition have been characterized via measuring terrestrial soils and atmospheric Hg samples. As summarized by Yin et al. (2018), terrestrial soils in general showed negative δ^{202}Hg (-1.8 ± 0.4‰, 2SD) and Δ^{199}Hg (-0.3 ± 0.1‰, 2SD), whereas atmospheric Hg samples showed relatively higher δ^{202}Hg (-1.2 ± 1.1‰, 2SD) and positive Δ^{199}Hg (0.4 ± 0.3‰, 2SD). Studies have utilized these signals to trace the sources of Hg in Chinese marginal sea sediments (Yin et al., 2015, 2018; Meng et al., 2019), and demonstrated that terrestrial-derived Hg is predominantly deposited in coastal/shelf areas, whereas Hg in open marine areas is primarily sourced from atmospheric deposition. Although these studies provided insights into the sources of Hg in marginal seas, their conclusions may not apply to deep oceans because hydrothermal vents may release a substantial amount of Hg in deep oceans (Bowman et al., 2016, 2019).

To date, however, the inputs and isotopic composition of Hg from hydrothermal vent fluids remains unclear. A previous study reported large variations of Hg ($0.8–2.0 \times 10^{-3}$ ng/g) in vent fluids from seafloor vent locations (Lamborg et al., 2006). Mercury emitted from vents may be removed by sulfides, due to the strong complexing of Hg with sulfur (German and Von Damm, 2003). This can be supported by the local enrichment of Hg in seafloor sediments in hydrothermal fields (HFs) in the East Pacific Rise (Dekov, 2007). Although some isotopic data (δ^{202}Hg: −0.37 to −0.01‰; Δ^{199}Hg: 0–0.04‰, n = 3) have been reported for seafloor solid samples (chimney piece and fluid precipitate) from the Guaymas Basin sea-floor rift in the Gulf of California (Sherman et al., 2009), the isotopic composition of Hg in seafloor sulfides on the seafloor hydrothermal systems, especially near mid-oceanic ridges, remains not well known. The isotopic composition of Hg in ancient hydrothermal ore deposits has been investigated by many studies, demonstrating rather consistent Hg isotopic signals (δ^{202}Hg: -0.47 ± 0.93‰; Δ^{199}Hg = 0.02 ± 0.13‰, 2SD; N = 102), although there are some outliers of the data (Smith et al., 2005, 2008; Sonke et al., 2010; Yin et al., 2013; 2016a; Tang et al., 2017; Xu et al., 2018). However, it is still unclear whether hydrothermal sulfides in modern seafloor hydrothermal systems have isotopically similar Hg compared to ancient hydrothermal ore deposits.

In this study, we for the first time report the isotopic composition of Hg in seafloor sulfides from two HFs (Duanqiao and Yuhuang) in the Southwest Indian Ridge (SWIR), which is an ultra-slow spreading ridge and is characterized by low melt production (Dick et al., 2003; Tao et al., 2020). The geological settings of the two HFs are quite different. The Yuhuang HF is a detachment faulting hydrothermal system (Liao et al., 2018), whereas the Duanqiao HF is a magma-related hydrothermal system (Yang, 2017; Jian et al., 2017a), indicating different models for hydrothermal circulation. Combining Hg and its isotopic signatures, we are able to better understand the fate of Hg in modern hydrothermal systems and give further constraints on Hg cycling in modern seawater.

2. GEOLOGIC SETTINGS

The SWIR, 8000 km long, forms the tectonic boundary between the Antarctic and African plates (Fig. 1), which represents over 10% of the total length of the global Mid-Ocean Ridge (Yang et al., 2017). Due to its oblique spreading, the SWIR has a slow spreading rate of approximately 0.7–1.6 cm/yr (Dick et al., 2003; Georgen et al. 2003). Large variations in the rift valley morphology, mantle compositions, magma activities and crustal thickness have been observed along the axis of the SWIR (Georgen et al., 2001; Sauter et al., 2009; Tao et al., 2014; Jian et al., 2017a,b).

Topography and geophysical studies indicate that intense hydrothermal activity is occurring along the SWIR. In the 49°E–52°E section of the SWIR, there are about 2.5 hydrothermal sites per 100 km, which is similar to that in the Mid-Atlantic Ridge at 36°N–38°N (Tao et al., 2012, 2014). Since 2007, at least seven HFs including the Duanqiao, Yuhuang, Longqi, Sudi, Baidi, Junhui and Baishen have been discovered in the central area of the SWIR (Tao et al., 2014). These HFs are situated between the

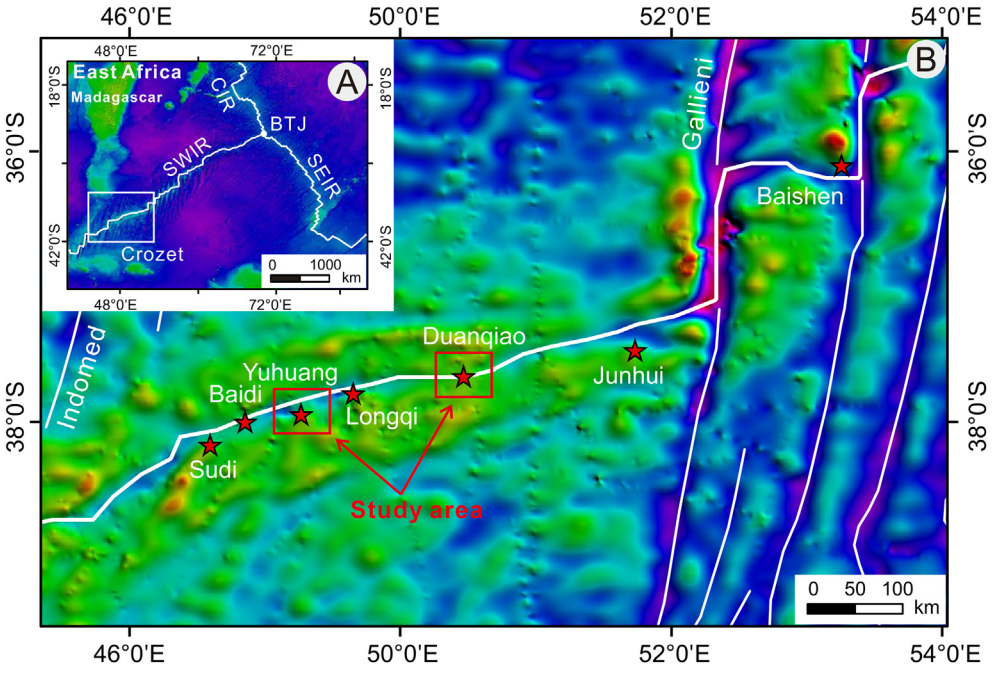

Fig. 1. Geological map of the Southwest Indian Ridge (based on Tao et al., 2012). The ridge axis (red line) and normal faults (white lines) are inferred from topography. Note: CIR, central Indian Ridge; SEIR, Southeast Indian Ridge; BTJ, Bouvet Triple Junction. (For interpretation of the references to colour in this figure legend, the reader is referred to the web version of this article.)

Indomed and Gallieni Fracture Zones (Fig. 1). Geophysical studies indicate that the thickness of the crust along the SWIR (~4 km) is much lesser than that of the neighboring areas (Baker and German, 2004). Studies also demonstrated that magma supply in this area has increased since 8–10 Ma. Crustal permeability and local magma supply played crucial roles in controlling the distribution of hydrothermal activities (Sauter et al., 2009; Tao et al., 2012).

The Duanqiao and Yuhuang HFs were selected as the study areas (Fig. 1). The Duanqiao HF, ~200 m × 125 m in size, is located on the segment 27 of the SWIR with a water depth of ~1700 m. This HF consists of hydrothermal vent chimneys, massive sulfides, opal, basalts, and metalliferous sediments (Yang et al., 2017). Sulfides in the Duanqiao HF mainly consist of high-temperature minerals such as chalcopyrite and pyrite (Yang, 2017). Beneath the center of segment 27, the basement rocks are mainly basalts with a crustal thickness of 10.2 km, suggesting a hot mantle or fertile melt underneath (Sauter et al., 2009; Niu et al., 2015). However, no active vents were discovered in the Duanqiao HF, suggesting that the hydrothermal activities ceased.

The Yuhuang HF, about 1000 m in diameter, is situated in segment 29 of the SWIR with a water depth of 1400–1600 m. It is about 7.5 km away from the ridge axis (Han et al., 2010; Han et al., 2015), and seated on a highland with an elevation of about 1500 m related to the bottom of the rift valley (Liao et al., 2018). The Yuhuang HF consists of sulfide chimneys and massive sulfides with an assemblage of relatively low-temperature mineral associations including abundant amorphous silica and sphalerite (Liao et al., 2018). No collapsed sulfide accumulations have been discovered, similar to the occurrence of zinc chimneys on the East Pacific Ridge (Paradis et al., 1988). In the Yuhuang HF, the basement rocks are predominantly basalts with minor ultramafic rocks, implying the development of detachment faults in this region (Liao et al., 2018). There are also no active vents discovered in the Yuhuang HF.

3. MATERIALS AND METHODS

3.1. Sample description and preparation

Eleven hand specimens, three from Duanqiao and eight from Yuhuang, were selected in this study. The hand specimens were collected using a TV-grab (grab system controlled via a TV camera) during the 34th cruise of Dayang Yihao from 2014 to 2015. Details of the samples were described previously (Yang et al., 2017; Liao et al., 2018) and are summarized in Table 1. Briefly, hand specimens from the Duanqiao HF are massive sulfide and chimney samples which mainly consist of pyrite and chalcopyrite with minor sphalerite and marcasite (Fig. 2 A, B and C). Hand specimens from the Yuhuang HF consist of massive sulfides (n = 5) and chimney samples (n = 3) (Fig. 2D, E and F), which are all predominantly composed of sphalerite, pyrite and amorphous silica with minor marcasite, chalcopyrite and pyrrhotite (Liao et al., 2018).

The hand specimens were carefully washed using deionized water and air-dried. Based on the results from the mineralogical studies (Yang, 2017; Liao et al., 2018), mineral grain-sizes are variable in different samples. Therefore, two techniques were used to treat the samples: (1) for large

Table 1
Major element concentrations, Hg and its isotope compositions of seafloor sulfides from the SWIR.

Sample No.	Ore types	Minerals	THg/(ng/g)	$\delta^{202/198}$Hg	Δ^{201}Hg	Δ^{199}Hg	Cu/(μg/g)	Fe/%	Zn/%
34Ⅳ-TVG-08-1-1P	Sulfide rich chimney	Py	4200	−0.47	0.03	0.07	890	43.7	0.9
34Ⅳ-TVG-08-1-1C		Ccp	350	−0.28	0.01	0.02	310,000	22.0	0.3
34Ⅳ-TVG-08-1-2P		Py	7000	−0.63	0.03	0.07	2000	39.1	0.3
34Ⅳ-TVG-08-2-1P		Py	2500	−0.33	0.06	0.03	2100	42.4	0.4
34Ⅳ-TVG-08-2-1P		Py	4300	−0.39	0.07	0.05	870	46.1	0.9
34Ⅳ-TVG-08-2-2P		Py	2500	−0.12	0.03	0.07	770	51.8	0.9
34Ⅳ-TVG-08-2-3P		Py	2600	−0.15	0.05	0.05	60	50.1	0.1
34Ⅳ-TVG-08-4-1P		Py	8100	−0.27	0.04	0.02	120	44.1	0.1
34Ⅳ-TVG-08-4-2P		Py	5800	−0.25	0.07	0.10	410	45.2	0.5
34Ⅳ-TVG-08-4-3P		Py	5800	−0.24	0.03	0.04	280	32.7	0.9
34Ⅱ-TVG-22-1-P	Silicified sulfide rich ore	Py	4100	−0.74	0.06	0.07	130	46.2	0.7
34Ⅱ-TVG-22-2-P	Zn-rich massive sulfide	Py	2400	−0.71	0.05	0.06	60	43.8	0.0
34Ⅱ-TVG-22-3-P	Silicified sulfide rich ore	Py	7200	−0.74	0.05	0.04	50	46.4	0.0
34Ⅱ-TVG-22-3-S		Sph	6000	−0.36	−0.01	−0.02	8800	3.3	47.2
34Ⅱ-TVG-22-4-P		Py	4900	−0.74	0.07	0.09	110	45.1	0.7
34Ⅱ-TVG-22-4-S		Sph	3810	−0.10	−0.05	−0.10	7300	2.9	42.8
34Ⅱ-TVG-22-5-P	Fe-rich massive sulfide	Py	5300	−0.87	0.00	0.07	570	37.5	0.6
34Ⅱ-TVG-22-7-P	Silicified sulfide rich ore	Py	7300	−0.68	0.04	0.10	250	44.0	0.3
34Ⅱ-TVG-23-3-S	Silicified sulfide chimney	Sph	2100	−0.65	0.01	0.05	8300	5.3	42.0
34II-TVG-22-2-3	Zn-rich massive sulfide	Sph-Md	1900	−0.67	−0.06	−0.05	4900	5.1	26.5
34II-TVG-22-2-4		Sph-Md	1000	−0.05	−0.10	−0.08	6100	6.0	24.6
34II-TVG-23-1-1	Silicified sulfide chimney	Py-Md	10,000	−0.94	0.01	0.02	50	3.0	0.9
34II-TVG-23-1-2		Sph-MD	1400	−0.26	0.00	−0.02	4900	9.1	47.7
34II-TVG-23-1-3		Sph-MD	830	−0.20	−0.05	−0.08	3700	8.0	32.5
34II-TVG-23-1-4		Py-Md	1500	−0.84	0.02	0.02	70	18.0	0.5
34II-TVG-23-1-5		Py-Md	44,000	−0.40	0.04	0.06	*	5.6	1.0
34II-TVG-23-1-6		Py-Md	2400	−0.50	−0.09	−0.05	100	6.5	2.1
34II-TVG-23-1-7		Py-Md	1800	−1.07	0.10	0.07	140	12.2	0.9
34II-TVG-23-1-8		Py-Md	440	−0.85	0.03	0.02	330	9.4	2.9
34II-TVG-23-1-9		Py-Md	10,000	−0.94	0.03	0.06	/	/	/
34II-TVG-23-1-10		Py-Md	1100	−0.35	0.03	0.04	*	25.8	1.8
34II-TVG-23-1-11		Py-Md	2700	−0.53	0.01	0.03	*	12.2	0.9
34IITVG-22-7-1	Silicified sulfide rich ore	Py-Md	9400	−0.64	0.02	0.03	210	35.6	0.1
34IITVG-22-7-2		Py-Md	7700	−0.94	0.08	0.13	100	40.3	0.0
34IITVG-22-7-3		Py-Md	2700	−1.23	0.19	0.20	460	22.0	0.1
34IITVG-22-7-4		Py-Md	2200	−0.90	0.15	0.11	420	26.6	0.1
34IITVG-22-7-5		Py-Md	960	−0.55	−0.02	0.04	1100	18.4	0.4
34IITVG-22-7-7		Py-Md	1500	−0.48	0.06	0.08	790	11.4	0.3
34IITVG-22-7-8		Py-Md	5900	−0.87	0.09	0.11	260	26.8	0.1
34IITVG-22-7-9		Py-Md	2000	−0.90	0.13	0.17	500	18.2	0.1
34IITVG-22-7-10		Py-Md	11,000	−1.03	0.05	0.08	/	/	/
34IITVG-22-7-11		Py-Md	3700	−0.87	0.06	0.09	/	/	/

Note: Py-MD, microdrilling sulfides mainly consist of pyrite; Sph-MD, microdrilling sulfides mainly consist of sphalerite; Py, handpicked pyrite; Ccp, handpicked chalcopyrite; Sph, handpicked sphalerite; "/" not measured; "*" below detection limit.

mineral grain-size sulfides, samples were handpicked under a binocular microscope after crushed into 40–60 mesh; (2) for small mineral grain-size sulfides, a micro-drilling system (Relion MSS IV; USA) was employed to collect samples from sulfide-rich points. The drill (NTI-Kahla Gmbn, Germany) is tungsten carbide-tipped and 2 mm in diameter, and was cleaned thoroughly using alcohol before drilling each point. The drill points are shown in Fig. 2.

3.2. Elemental concentration and Hg isotope composition analysis

To ascertain the dominant sulfide minerals in the drilled samples, ~ 10 mg of each drilled sample was digested with 1 mL aqua regia at 120 °C for 120 min. Then, Zn, Fe and Cu concentrations were measured using a Varian Vista MPX Inductively coupled plasma-optical emission spectrometry (ICP-OES) at the State Key Laboratory of Ore Deposit Geochemistry, Institute of Geochemistry, Chinese Academy of Sciences. Internal laboratory standard solutions (BWB2070-2016, BWB2068-2016 and CLCU2-2Y) were used to calibrate the concentration of Zn, Fe and Cu in digest solutions, respectively. Standard reference material, GBW 07237 (Zn ores) was used for quality control. The recoveries of Zn, Fe and Cu in GBW 07237 were between 95 and 105% (n = 3).

About 50 mg of mineral and drilled samples were digested with 5 mL aqua regia ($HCl/HNO_3 = 3$, v/v) at

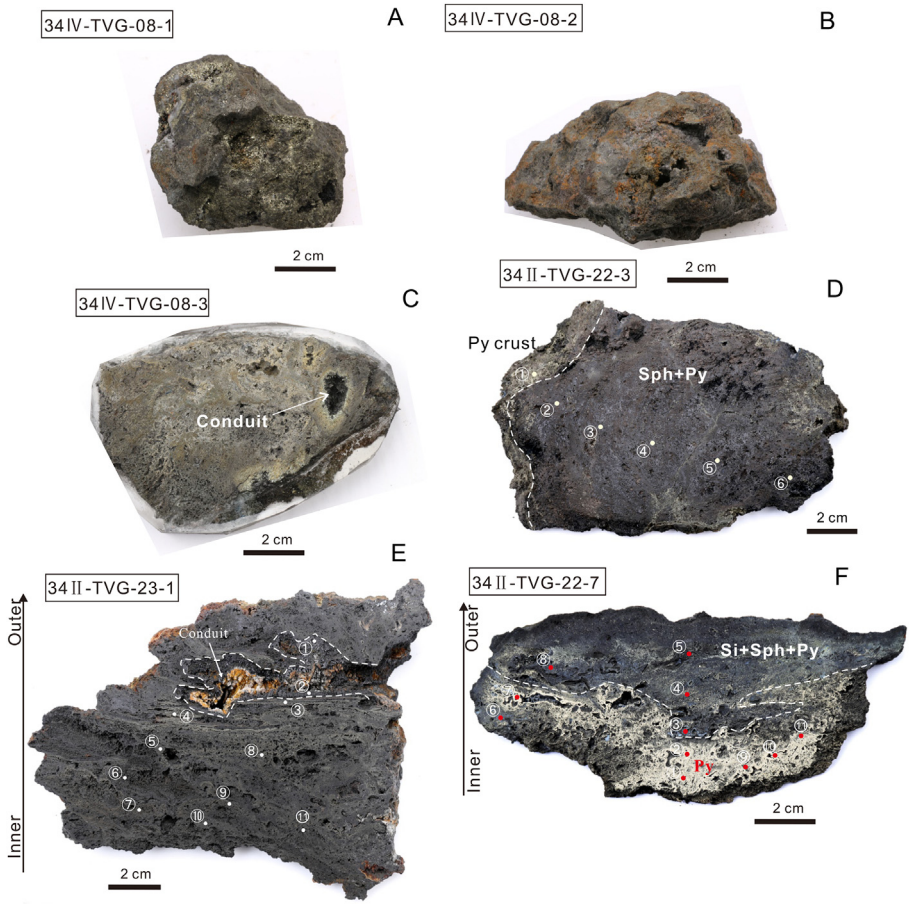

Fig. 2. Photographs of selected hand specimens collected from the Duanqiao and Yuhuang hydrothermal fields. Photographs A, B and C illustrate massive sulfide and sulfide-rich chimney pieces from Duanqiao, with pyrite and chalcopyrite as the predominant minerals; Photograph D depicts a Zn-rich massive sulfide sample with a pyrite crust; Photograph E shows a silicified chimney piece with a fluid conduit. The sample can be divided into two layers on the basis of the mineral associations and sphalerite grown on the conduit walls, as coarse crystals; Photograph F shows a pyritic massive sulfide with a siliceous crust and the sample can be divided into two layers, amorphous Si is a predominant material on the top and pyrite is a predominant mineral on the bottom.

95 °C for 6 h. Standard reference materials, MESS-2 (marine sediment) was prepared in the same way as the samples. Mercury concentrations in digested solutions were measured using an MA-2000 mercury analyzer at the United States Geological Survey (USGS) Mercury Research Lab, following a previous method (Lepak et al., 2015). Recoveries of Hg in MESS-2 were between 90 and 110% (n = 3).

The digest solutions were diluted to 0.5 ng/mL Hg with acid matrices of 10–20%, and measured with a Neptune Plus multiple collector inductively coupled plasma mass spectrometer (MC-ICP-MS) at the University of Wisconsin-Madison, following a previous method (Yin et al., 2016b). The $\delta^{202}Hg$, $\Delta^{199}Hg$, $\Delta^{200}Hg$, and $\Delta^{201}Hg$ values were calculated relative to NIST SRM 3133, following a standard-sample-standard bracketing protocol (Blum and Bergquist, 2007). Mercury concentrations and acid matrices in the bracketing NIST SRM 3133 solutions were matched within 10% with the neighbouring samples. Duplicate UM-Almadén secondary solutions (0.5 ng/mL Hg) were prepared using 10% (v/v) aqua regia, and measured in every five samples. The sensitivity of ^{202}Hg was ~1.2 V per ppb Hg during analysis. The measured values for UM-Almadén ($\delta^{202}Hg = -0.55 \pm 0.09‰$; $\Delta^{201}Hg = -0.05 \pm 0.03‰$; $\Delta^{200}Hg = -0.01 \pm 0.02‰$; $\Delta^{199}Hg = -0.02 \pm 0.03‰$; 2SD, n = 10) and MESS-2 ($\delta^{202}Hg = -2.10 \pm 0.10‰$; $\Delta^{201}Hg = -0.01 \pm 0.03‰$; $\Delta^{200}Hg = 0.01 \pm 0.02‰$; $\Delta^{199}Hg = 0.04 \pm 0.05‰$; 2SD, n = 3) agreed well with previous results (Blum and Bergquist, 2007; Lepak et al., 2015; Yin et al., 2016b).

4. RESULTS

Elemental (Hg, Zn, Fe and Cu) concentrations and Hg isotope compositions of the samples are summarized in Table 1. In the Yuhuang HF, the drilled samples showed high Fe and Zn concentrations levels of 3.0–40.3% and 0–47.7%, respectively, indicating that Fe and Zn sulfides (e.g., pyrite and sphalerite) are the predominant minerals in these samples. In contrast, Cu showed much lower concentrations (5.0×10^1–6.1×10^3 μg/g), indicating that Cu sulfides (e.g., chalcopyrite) are minor (Table 1).

Hg concentrations in hand-picked minerals from the Duanqiao and the Yuhuang HFs range from 3.5×10^2 to

8.1×10^3 ng/g and from 4.4×10^2 to 4.4×10^4 ng/g, respectively, within the range reported for hydrothermal ore deposits (6.3×10^2–1.8×10^5 ng/g; Yin et al., 2016a). As shown in Fig. 3A and Table 1, except one sample (34Ⅲ-TVG-23-1-5) which showed the highest Hg concentration of 4.4×10^4 ng/g, most drilled samples have Hg concentrations (4.4×10^2–1.1×10^4 ng/g) that are similar to handpicked samples (3.5×10^2–8.1×10^3 ng/g). Regarding the drilled samples (finer-grained) and handpicked pure mineral samples, there are no significant correlations between Hg and Fe and between Hg and Zn in seafloor sulfides from either the Duanqiao or the Yuhuang HFs (Table 1). Regarding handpicked minerals (coarser-grained) in the Duanqiao HF, pyrite showed the highest Hg concentrations (2.5×10^3–8.1×10^3 ng/g, n = 9), followed by chalcopyrite (3.5×10^2 ng/g, n = 1). In the Yuhuang HF, pyrite (4.4×10^2–4.4×10^4 ng/g, n = 25) shows a wider range of Hg concentrations than sphalerites (8.3×10^2–6.0×10^3 ng/g, n = 7) (Fig. 3A).

δ^{202}Hg values of all the samples range from −1.23 to −0.05 ‰ with a mean value of -0.59 ± 0.61‰ (2SD, n = 42) (Fig. 3B), similar to previous results on VMS ore deposits in China (−80.84 to −0.13‰; -0.52 ± 0.47‰; 2SD, n = 14) (Yin et al., 2016a) and modern vent chimneys from Guaymas Basin, México (−0.37 to −0.01‰; -0.23 ± 0.39‰; 2SD, n = 3) (Sherman et al., 2009). Sulfides from the Yuhuang HF have a mean value of -0.68 ± 0.59‰ (n = 32; 2SD), which is overlapped with that of the Duanqiao HF (-0.31 ± 0.30‰; n = 10, 2SD). Within the same hand specimen, it is interesting that pyrites always showed slightly lower δ^{202}Hg values than sphalerites and chalcopyrite (Fig. 4).

Unlike δ^{202}Hg, the Δ^{199}Hg values showed a significant difference between the two HFs. Sulfides from the Duanqiao HF showed insignificant Hg-MIF with Δ^{199}Hg values varying from 0.02 to 0.10‰ (mean = 0.05 ± 0.05‰, 2SD; n = 10); the Yuhuang HF showed small but significant Hg-MIF with the variation of Δ^{199}Hg (−0.10 to 0.20‰, mean = 0.05 ± 0.14‰, 2SD; n = 32) about 6 times higher than the analytical uncertainty (±0.05‰, 2SD). A significantly positive correlation between Δ^{199}Hg and Δ^{201}Hg ($p < 0.01$, $R^2 = 0.89$), with Δ^{199}Hg/Δ^{201}Hg of 0.97 ± 0.08 (2SE), is observed for the Yuhuang samples (Fig. 5 A and B), which is consistent with that reported during aqueous Hg(II) photochemical reduction (Bergquist and Blum, 2007). A significantly negative correlation ($p < 0.01$, $R^2 = 0.64$) between δ^{202}Hg and Δ^{199}Hg was observed in the Yuhuang samples (Fig. 5A).

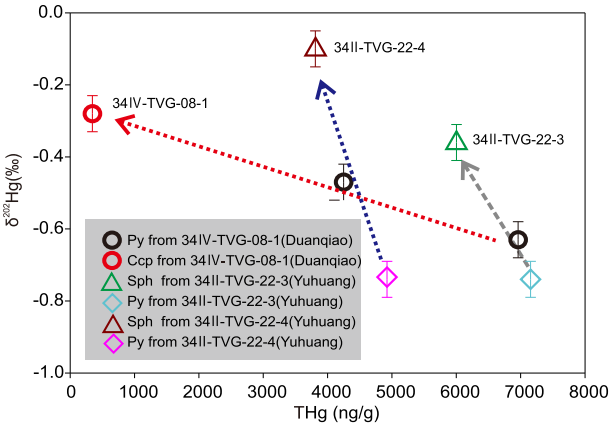

Fig. 4. Hg concentrations versus δ^{202}Hg values in coexisting sulfide mineral pairs from the Duanqiao and the Yuhuang HFs.

5. DISCUSSION

5.1. Mercury occurrence in HF sulfides

Mercury in hydrothermal systems may be present as (1) adsorbed form on mineral surface, (2) native Hg or independent Hg minerals and (3) isomorphic substitution (Rytuba, 2003; Dekov, 2007; Prol-Ledesma et al., 2002; Schwartz 1997; Stoffers et al., 1999; Xu et al., 2018). It is unlikely that adsorbed Hg is the dominant form of Hg in sulfides, because Hg is readily complexed with sulfur. Microscopic observations did not show native Hg or any Hg minerals (e.g., cinnabar) in the studied samples (Liao et al., 2018, 2019). Several studies have shown that Hg is normally present replacing Zn(II), Pb(II), Sb(II) and Fe (II) by Hg(II) (Schwartz 1997; Rytuba 2003). Isomorphic

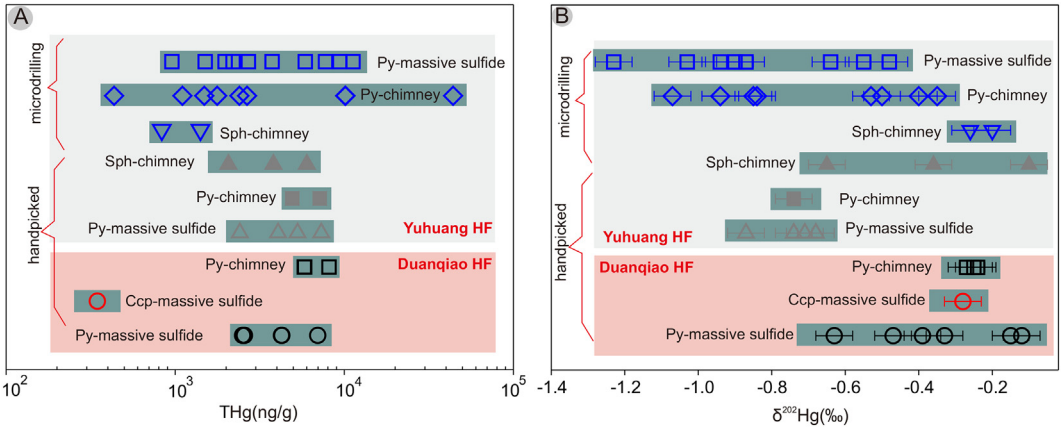

Fig. 3. Variations of THg (A) and δ^{202}Hg (B) in sulfides from the Duanqiao and Yuhuang HFs.

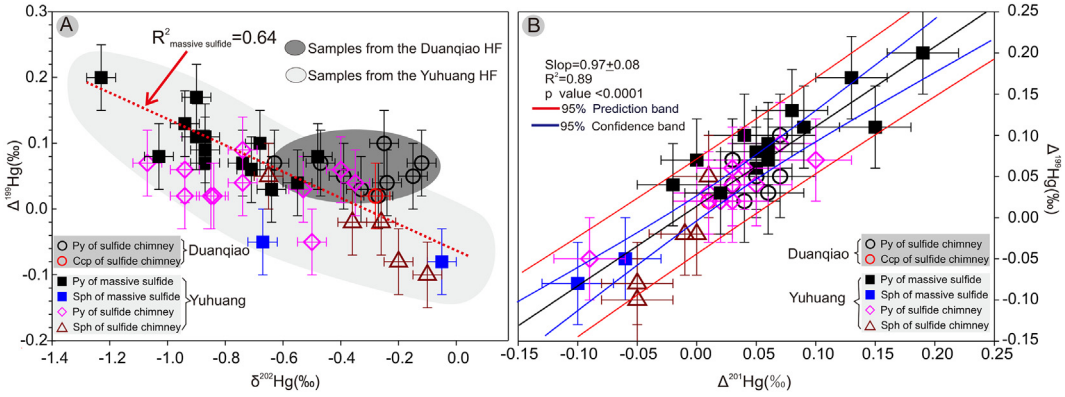

Fig. 5. (A) δ^{202}Hg versus Δ^{199}Hg in sulfides; (B) Δ^{201}Hg versus Δ^{199}Hg in sulfides from the Duanqiao and Yuhuang hydrothermal fields. Error bars are based on replicate analyses of procedural standards.

substitution of Fe(II) and Zn(II) by Hg(II) is most likely the form of Hg fixation in our samples, because of the high abundance of Fe and Zn in these samples.

5.2. Mass-dependent fractionation of Hg isotopes

In previous studies, it has been shown that magmatic processes and the release of Hg from source rocks under high-temperature conditions can only generate limited or no Hg-MDF (<±0.5‰) (Smith et al. 2008; Sherman et al. 2009). However, redox reactions, boiling of hydrothermal fluids and mineral precipitation can result in significant Hg-MDF (Smith et al., 2005, 2008; Tang et al., 2017). Large variations of δ^{202}Hg (up to >5‰) have been observed in two fossil hydrothermal systems in the US., which have been ascribed to the boiling of hydrothermal fluids and associated loss of isotopically light Hg(0) at the surface of the hydrothermal system (Smith et al., 2005). In hydrothermal deposits where boiling is not common, however, δ^{202}Hg show narrow ranges; this can be seen from the small variations of δ^{202}Hg in a Mississippi Valley-type deposit in the US (~1.2 ‰; according to Smith (2010)) and two sediment-hosted Pb-Zn deposits in China (Lanuoma: ~1.6‰; Cuona: ~1.2‰; Xu et al., 2018). In the present study, the small variations of δ^{202}Hg for the Duanqiao (−0.63 to −0.12‰) and Yuhuang HFs (−1.23 to −0.05‰) suggest the loss of Hg(0) vapor from hydrothermal fluids may be limited in both HFs.

A recent study by Tang et al. (2017) showed that Hg-MDF may occur during the formation of sulfide minerals, for instance, they reported slightly lower δ^{202}Hg in the early-formed sphalerites than in late-formed pyrites in the Jinding Pb-Zn deposit (Tang et al., 2017). This is consistent with previous studies which also showed that lighter isotopes of other metals (e.g., Fe, Zn and Cd) can be preferentially enriched in early-formed minerals (Gagnevin et al., 2012; Zhu et al., 2017). In this study, we observe slightly lower δ^{202}Hg in pyrites (−0.74 to −0.47‰) compared with sphalerites and chalcopyrite (−0.36 to −0.10‰) in the same hand specimen (e.g., 34Ⅱ-TVG-22-4-P and 34Ⅱ-TVG-22-4-S; see Table 1; Fig. 4), which indicate that Hg-MDF may have occurred during the formation of the studied sulfide minerals. However, no systematic differences in δ^{202}Hg can be found between sulfide minerals from other hand specimens. More likely, small but statistically significant offsets in δ^{202}Hg between the two sites could be due to mixing fluids containing Hg with distinct δ^{202}Hg signals (Fig. 5A) (see discussion below).

5.3. Mass-independent fractionation of Hg isotopes

As hydrothermal processes induce limited Hg-MIF, Δ^{199}Hg and Δ^{201}Hg values have been directly used to trace multiple sources of Hg in hydrothermal deposits (Yin et al., 2016a; Xu et al., 2018). Studies have suggested that nuclear volume effect (NVE) and the magnetic isotope effect (MIE) are the two potential mechanisms that generate Hg-MIF. NVE and MIE can be distinguished according to their Δ^{199}Hg/Δ^{201}Hg ratios. NVE occurs during several processes such as elemental Hg(0) evaporation (Estrade et al., 2009; Ghosh et al., 2013) and dark Hg(II) reduction (Zheng and Hintelmann, 2010), which are associated with Δ^{199}Hg/Δ^{201}Hg of ~1.6 to ~1.7; MIE mainly occurs during photochemical processes such as aqueous Hg(II) photo-reduction and photo-degradation of MeHg, with Δ^{199}Hg/Δ^{201}Hg ratios of 1.0 and 1.3, respectively (Bergquist and Blum, 2007; Zheng and Hintelmann, 2010). Hg-MIF has been widely observed in "environmental reservoirs" on Earth's surface, such as soil/sediments, water/snow, plants and atmospheric Hg samples, with Δ^{199}Hg/Δ^{201}Hg ratios of 1.0, suggesting that Hg(II) photo-reduction is the major process causing Hg-MIF in natural samples (Blum et al., 2014).

In this study, no Hg-MIF was observed in the Duanqiao HF (Δ^{199}Hg: 0.02–0.10‰), which suggests that Hg in this HF is of syngenetic origin because magmatic/mantle materials are characterized by the absence of MIF (Δ^{199}Hg ~ 0) (Sherman et al., 2009; Smith et al., 2008). However, small but significant Hg-MIF was observed in the Yuhuang HF (Δ^{199}Hg: −0.10 to 0.20‰). This suggests that syngenetic Hg is not the single source of Hg in the Yuhuang HF. The positive correlation between Δ^{199}Hg and Δ^{201}Hg (Δ^{199}Hg/Δ^{201}Hg = 0.97 ± 0.08; 2SE) observed in the Yuhuang sulfide samples suggests that some Hg-MIF in

the Yuhuang HF was triggered by Hg(II) photo-reduction prior to precipitation into sulfides. Pronounced Hg-MIF signals have been recently observed in hydrothermal sulfide deposits, which have been interpreted as an inheritance of epigenetic Hg via sedimentation and hydrothermal leaching (Sonke et al., 2010; Yin et al., 2016a; Xu et al., 2018). Here, we hypothesize that besides receiving Hg from magmatic/mantle materials under the seafloor, the Yuhuang HF may also have received Hg from seawater or seabed sediments. The majority of samples from Yuhuang have Δ^{199}Hg values within 0 ± 0.1‰ (Fig. 6), indicating syngenetic Hg as the dominant source. However, the rest of the samples show positive Δ^{199}Hg values (>0.1‰, Fig. 6). Previous studies have observed positive Δ^{199}Hg values in both filtered seawater samples (0.21 ± 0.13‰; Štrok et al., 2015) and marine sediments (0.14 ± 0.18‰; Gehrke et al., 2009; Yin et al., 2015; Meng et al., 2019). The positive Δ^{199}Hg values in marine sediments are inherited from the seawater through the scavenge of seawater Hg by sediment particles (Gehrke et al., 2009; Grasby et al., 2017; Yin et al., 2015, 2017; Wang et al., 2019). The positive Δ^{199}Hg of Yuhuang samples would thus be directly inherited from seawater and marine sediments. However, due to the similarity of Hg-MIF between seawater and marine sediments (Fig. 6), it is not realistic to distinguish the contribution of Hg from these two sources by the simple mass balance calculation. We hypothesized that compared to seawater, sediments may play a less important role in contributing Hg to the Yuhuang seafloor sulfides, due to the following reasons: (1) Sediments were not or rarely found in most areas, as seafloor sulfides and igneous rocks can be directly observed (Fig. S1). Considering its long distance from the continent (Fig. 1A), we would not expect a significant accumulation of sediments in Yuhuang; (2) According to previous studies (Liao et al., 2018, 2019), seafloor sulfides in Yuhuang are directly overlaid on igneous rocks and then covered by sediments. In this case, sediments are younger

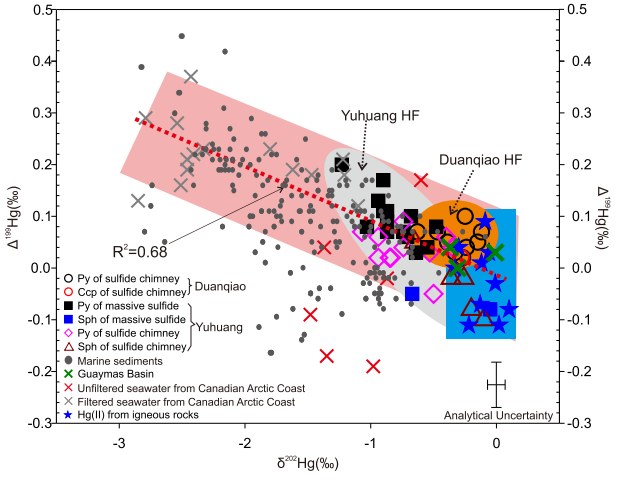

Fig. 6. δ^{202}Hg versus Δ^{199}Hg in sulfides from the Yuhuang and Duanqiao hydrothermal fields. Seawater data are based on Strok et al., (2015), and marine sediments data are cited from Gehrke et al. (2009), Yin et al. (2015) and Meng et al. (2019); Data for magmatic/mantle are based on Sherman et al. (2009) and Zambardi et al. (2009).

than seafloor sulfides and unlikely to serve as a major source of Hg to seafloor sulfides, which were precipitated from the hydrothermal fluids that circulated from the deep oceanic crust (Cave et al., 2002; Tivey, 2007). Many studies on hydrothermal systems from sediment-starved mid-ocean ridges exclude sediments as a major source of seafloor sulfides (e.g., Spivack and Edmond, 1987; Ono et al., 2007; Tivey, 2007). In this study, we roughly estimated that about 10% to 95% of Hg was derived from seawater for the Yuhuang samples with positive Δ^{199}Hg values (0–0.2‰), by dividing the Δ^{199}Hg of the samples by that of seawater (0.21 ± 0.13‰; Štrok et al., 2015). However, it needs to be cautioned our estimates may have large uncertainties, as seawater Hg-MIF may vary at different locations.

5.4. Implications for models of the Duanqiao and Yuhuang hydrothermal fields

The difference in Hg sources, as illustrated by Hg-MIF signals in sulfides, enables us to further establish two

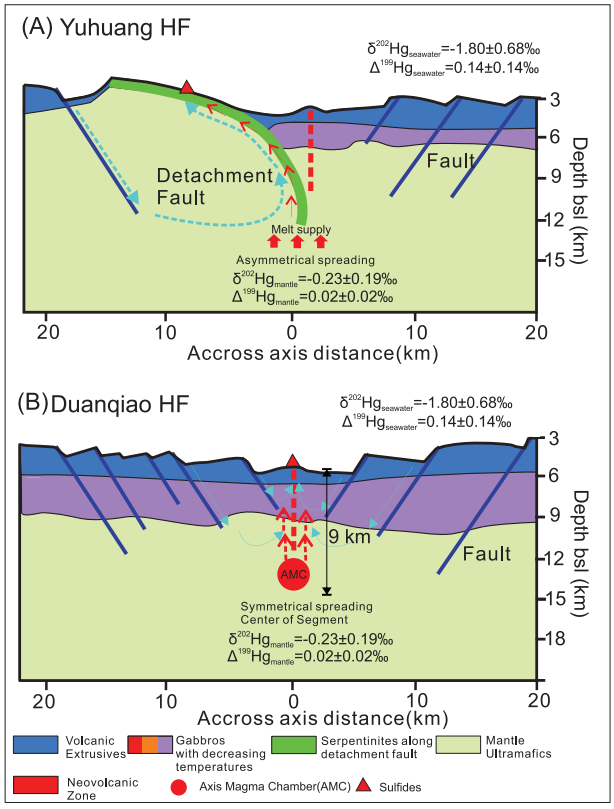

Fig. 7. Conceptual models showing the geological settings and fluid cycling of the Duanqiao and Yuhuang HFs (modified from Fouquet et al., 2010; Data sources: Štrok et al., 2015; Sherman et al., 2009). Note that bsl means below sea level. The depth of the detachment fault at Yuhuang remains unknown. According to previous studies, the detachment faults in Longqi HF (Fig. 1B) at SWIR can be traced up to 13 ± 2 km below the seafloor (Tao et al., 2020). As Yuhuang is nearby to Longqi, Yuhuang should share some similarities to Longqi. We therefore assumed a similar depth of the detachment fault (~13 km) to the Yuhuang HF, however, this number may not be precise and needs to be cautioned.

models for the Duanqiao and Yuhuang HFs. The absence of Hg-MIF in the Duanqiao HF suggests that magmatic/mantle materials are the dominant source of Hg in this HF. This can be supported by the fact that the Duanqiao HF is situated on the axis of the SWIR, where an axial magma chamber (AMC) exists ~4 to 9 km below the seafloor (Baker et al., 1996; Sauter et al., 2009; Niu et al., 2015; Yang, 2017; Jian et al., 2017a; Sun et al., 2018; Yue et al., 2019). As shown in Figs. 6 and 7, the AMC directly serves as a source of materials to the formation of the Duanqiao HF. Therefore, the Duanqiao HF is a typical volcanogenic massive sulfide (VMS) deposit, which are commonly related to deep-seated intrusions of magmatic materials in submarine divergent margins (e.g. Mid-Ocean Ridges). According to Yin et al. (2012), mercury is found in abundance in VMS deposits. Some metals in VMS deposits are incompatible elements which are transported to VMS deposits via convection of hydrothermal fluids. The heat supplied by the magma chamber (which sits below the volcanic edifice) can enrich the hydrothermal fluid in sulfur and metal ions. Submarine volcanism and chemical sedimentation may provide a favorable setting for Hg transport and deposition. According to Yin et al. (2016a), VMS deposits show similar Hg isotopic compositions (δ^{202}Hg: −0.84 to −0.13‰; Δ^{199}Hg: −0.06 to 0.06‰; n = 14) to the Duanqiao samples (δ^{202}Hg: −0.12 to −0.63‰; Δ^{199}Hg: 0.02–0.10‰; n = 10).

Unlike Duanqiao, the Yuhuang HF is a detachment-fault related hydrothermal system which is >7.5 km away from the ridge axis (Fig. 1; Liao et al., 2018). Magmatic Hg remains the major source of Hg in the Yuhuang HF, but it may have played a relatively less important role compared with the Duanqiao HF. It is believed that magmatic activities near Mid-Ocean Ridges not only serve as an energy source that drives the hot and sulfur-rich brines (largely evolved seawater) mixing with the cooler, unmodified seawater, but also release of ore-bearing hydrothermal fluids into ocean water, resulting in the formation and precipitation of Hg-rich sulfides onto the seafloor (Fig. 7A and B).

6. CONCLUSIONS

This study evidenced extreme enrichment of Hg in sulfides collected from the Yuhuang and Duanqiao HFs and confirmed that these HFs can be significant contributors to the deep ocean environment. For both HFs, Hg seems to mainly occur in the solid solution of sulfides, through the incorporation of Hg(II) in Fe(II) and Zn(II) sulfides. The observation of distinct Hg isotopic signals between the Yuhuang and Duanqiao HFs suggests that Hg sources are different for the two HFs. The Yuhuang HF is characterized by a narrow range of δ^{202}Hg (−0.84 to −0.13‰) and the absence of Hg-MIF signals (Δ^{199}Hg: −0.06 to 0.06‰), suggesting magmatic/mantle Hg as a dominant source. The Duanqiao HF, however, showed large ranges of δ^{202}Hg (−1.23 to −0.05‰) and Δ^{199}Hg (−0.10 to 0.20‰), indicating magmatic/mantle Hg is not the sole source. The significant Hg-MIF observed in Duanqiao suggests a substantial contribution of Hg from seawater. This study, therefore, sheds some new lights on understanding the source of Hg under the seafloor.

Declaration of Competing Interest

The authors declare that they have no known competing financial interests or personal relationships that could have appeared to influence the work reported in this paper.

ACKNOWLEDGEMENTS

This work was supported by the National Key R&D Program of China (2018YFC0309902), and National Natural Science Foundation of China (41773012). Wisconsin State Laboratory of Hygiene is acknowledged for providing lab facilities. Referees are acknowledged for reviewing this paper.

APPENDIX A. SUPPLEMENTARY MATERIAL

Supplementary data to this article can be found online at https://doi.org/10.1016/j.gca.2020.05.008.

REFERENCES

Amos H. M., Jacob D. J., Kocman D., Horowitz H. M., Zhang Y., Dutkiewicz S., Horvat M., Corbitt E. S., Krabbernhoft D. P. and Sunderland E. M. (2014) Global biogeochemical implications of mercury discharges from rivers and sediment burial. *Environ. Sci. Technol.* **48**(16), 9514–9522.

Baker E. T., Chen Y. J. and Morgan J. P. (1996) The relationship between near-axis hydrothermal cooling and the spreading rate of mid-ocean ridges. *Earth Planet. Sci. Lett.* **142**(1–2), 137–145.

Baker E. T. and German C. R. (2004) On the global distribution of hydrothermal vent fields. *Mid-Ocean Ridges: Hydrothermal Interactions Between the Lithosphere and Oceans. Geophys. Monogr. Ser.* **148**, 245–266.

Bergquist B. A. and Blum J. D. (2007) Mass-dependent and-independent fractionation of Hg isotopes by photoreduction in aquatic systems. *Science* **318**(5849), 417–420.

Bergquist B. A. and Blum J. D. (2009) The odds and evens of mercury isotopes: applications of mass-dependent and mass-independent isotope fractionation. *Elements* **5**(6), 353–357.

Blum J. D. and Bergquist B. A. (2007) Reporting of variations in the natural isotopic composition of mercury. *Anal. Bioanal. Chem.* **388**(2), 353–359.

Blum J. D., Sherman L. S. and Johnson M. W. (2014) Mercury isotopes in earth and environmental sciences. *Annu. Rev. Earth Planet. Sci.* **42**, 249–269.

Bowman K. L., Hammerschmidt C. R., Lamborg C. H., Swarr G. J. and Agather A. M. (2016) Distribution of mercury species across a zonal section of the eastern tropical South Pacific Ocean (US GEOTRACES GP16). *Mar. Chem.* **186**, 156–166.

Bowman K. L., Lamborg C. H. and Agather A. M. (2019) A global perspective on mercury cycling in the ocean. *Sci. Total Environ.*. https://doi.org/10.1016/j.scitotenv.2019.136166.

Cave R. R., German C. R., Thomson J. and Nesbitt R. W. (2002) Fluxes to sediments underlying the Rainbow hydrothermal plume at 36 14′ N on the Mid-Atlantic Ridge. *Geochim. Cosmochim. Acta* **66**(11), 1905–1923.

Dekov V. M. (2007) Native Hg_{liq} in the metalliferous sediments of the East Pacific Rise (21° S). *Mar. Geol.* **238**(1–4), 107–113.

Dick H. J., Lin J. and Schouten H. (2003) An ultraslow-spreading class of ocean ridge. *Nature* **426**(6965), 405.

Estrade N., Carignan J., Sonke J. E. and Donard O. F. (2009) Mercury isotope fractionation during liquid–vapor evaporation experiments. *Geochim. Cosmochim. Acta* **73**(10), 2693–2711.

Fouquet Y., Cambon P., Etoubleau J., Charlou J. L., OndréAs H., Barriga F. J. A. S., Cherkashov G., Semkova T., Poroshina I., Bohn M., Donval J. P., Henry K., Murphy P. and Rouxel O. (2010) Geodiversity of hydrothermal processes along the Mid-Atlantic Ridge and ultramafic-hosted mineralization: a new type of oceanic Cu-Zn-Co-Au volcanogenic massive sulfide deposit. *Diversity Hydrothermal Syst. Slow Spread. Ocean Ridges* **188**, 321–367.

Gagnevin D., Boyce A. J., Barrie C. D., Menuge J. F. and Blakeman R. J. (2012) Zn, Fe and S isotope fractionation in a large hydrothermal system. *Geochim. Cosmochim. Acta* **88**, 183–198.

Gehrke G. E., Blum J. D. and Meyers P. A. (2009) The geochemical behavior and isotopic composition of Hg in a mid-Pleistocene western Mediterranean sapropel. *Geochim. Cosmochim. Acta* **73**(6), 1651–1665.

Georgen J. E., Lin J. and Dick H. J. (2001) Evidence from gravity anomalies for interactions of the Marion and Bouvet hotspots with the Southwest Indian Ridge: effects of transform offsets. *Earth Planet. Sci. Lett.* **187**(3–4), 283–300.

Georgen J. E., Kurz M. D., Dick H. J. and Lin J. (2003) Low $^{3}He/^{4}He$ ratios in basalt glasses from the western Southwest Indian Ridge (10°-24° E). *Earth Planet. Sci. Lett.* **206**(3), 509–528.

German C. and Von Damm K. L. (2003) Hydrothermal processes. In The Treatise on Geochemistry, vol. 6 (eds. K. K. Turekian and H. D. Holland). Elsevier, pp. 181–222.

Ghosh S., Schauble E. A., Couloume G. L., Blum J. D., Hurley J. P. and Bergquist B. A. (2013) Estimation of nuclear volume dependent fractionation of mercury isotopes in equilibrium liquid–vapor evaporation experiments. *Chem. Geol.* **336**, 5–12.

Grasby S. E., Shen W., Yin R., Gleason J. D., Blum J. D., Lepak R. F., Hurley J. P. and Beauchamp B. (2017) Isotopic signatures of mercury contamination in latest Permian oceans. *Geology* **45**(1), 55–58.

Gworek B., Bemowska-Kałabun O., Kijeńska M. and Wrzosek-Jakubowska J. (2016) Mercury in marine and oceanic waters—a review. *Water Air Soil Pollut.* **227**(10), 371.

Han X. Q., Wu G. H., Cui R., Qiu Z. Y., Deng X. M., Wang Y., Dy S. P. O. and Leg C. (2010) Discovery of a hydrothermal sulfide deposit on the Southwest Indian Ridge at 49.2°E. *American Geophysical Union, Fall Meeting, S21C-S1531C*.

Han X. Q., Wang Y. J., Qiu Z. Y., Liu Y. and Qiu B. B. (2015) Discovery and mineralization features of the Yuhuang-1 hydrothermal field on Southwest Indian Ridge. *Acta Mineralogica Sinica* **35**(S1), 1141–1142 (In Chinese with English abstract).

Jian H. C., Singh S. C., Chen Y. J. and Li J. (2017a) Evidence of an axial magma chamber beneath the ultraslow-spreading Southwest Indian Ridge. *Geology* **45**(2), 143–146.

Jian H. C., Chen Y. J., Singh S. C., Li J. B., Zhao M. H., Ruan A. G. and Qiu X. L. (2017b) Seismic structure and magmatic construction of crust at the ultraslow-spreading Southwest Indian Ridge at 50°28'E. *J. Geophys. Res. Solid Earth* **122**(1), 18–42.

Kim K. H., Kabir E. and Jahan S. A. (2016) A review on the distribution of Hg in the environment and its human health impacts. *J. Hazard. Mater.* **306**, 376–385.

Lamborg C. H., Von Damm K. L., Fitzgerald W. F., Hammerschmidt C. R. and Zierenberg R. (2006) Mercury and monomethylmercury in fluids from Sea Cliff submarine hydrothermal field, Gorda Ridge. *Geophys. Res. Lett.* **33**, L17606.

Lepak R. F., Yin R., Krabbenhoft D. P., Ogorek J. M., DeWild J. F., Holsen T. M. and Hurley J. P. (2015) Use of stable isotope signatures to determine mercury sources in the Great Lakes. *Environ. Sci. Technol. Lett.* **2**(12), 335–341.

Liao S., Tao C., Li H., Barriga F. J. A. S., Liang J., Yang W., Yu J. Y. and Zhu C. (2018) Bulk geochemistry, sulfur isotope characteristics of the Yuhuang-1 hydrothermal field on the ultraslow-spreading Southwest Indian Ridge. *Ore Geol. Rev.* **96**, 13–27.

Liao S., Tao C., Zhu C., Li H., Li X., Liang J., Yang W. and Wang Y. (2019) Two episodes of sulfide mineralization at the Yuhuang-1 hydrothermal field on the Southwest Indian Ridge: insight from Zn isotopes. *Chem. Geol.* **507**, 54–63.

Mason R. P., Choi A. L., Fitzgerald W. F., Hammerschmidt C. R., Lamborg C. H., Soerensen A. L. and Sunderland E. M. (2012) Mercury biogeochemical cycling in the ocean and policy implications. *Environ. Res.* **119**, 101–117.

Meng M., Sun R. Y., Liu H. W., Yu B., Yin Y. G., Hu L. G., Shi J. B. and Jiang G. B. (2019) An integrated model for input and migration of mercury in Chinese coastal sediments. *Environ. Sci. Technol.* **53**(5), 2460–2471.

Niu X., Ruan A., Li J., Minshull T. A., Sauter D., Wu Z., Qiu X., Zhao M., Chen Y. J. and Singh S. (2015) Along-axis variation in crustal thickness at the ultraslow spreading Southwest Indian Ridge (50° E) from a wide-angle seismic experiment. *Geochem. Geophys. Geosyst.* **16**(2), 468–485.

Ono S., Shanks, III, W. C., Rouxel O. J. and Rumble D. (2007) S-33 constraints on the seawater sulfate contribution in modern seafloor hydrothermal vent sulfides. *Geochim. Cosmochim. Acta* **71**(5), 1170–1182.

Paradis S., Jonasson I. R., Le Cheminant G. M. and Watkinsons D. H. (1988) Two zinc-rich chimneys from the Plume Site, southern Juan de Fuca Ridge. *The Can. Mineral.* **26**(3), 637–654.

Pirrone N., Cinnirella S., Feng X., Finkelman R. B., Friedli H. R., Leaner J., Mason R., Mukherjee A. B., Stracher G. B. and Streets D. G. (2010) Global mercury emissions to the atmosphere from anthropogenic and natural sources. *Atmos. Chem. And Phys.* **10**, 5951–5964.

Rytuba J. J. (2003) Mercury from mineral deposits and potential environmental impact. *Environ. Geol.* **43**, 326–338.

Sauter D., Cannat M., Meyzen C., Bezos A., Patriat P., Humler E. and Debayle E. (2009) Propagation of a melting anomaly along the ultraslow Southwest Indian Ridge between 46° E and 52° 20′ E: interaction with the Crozet hotspot? *Geophys. J. Int.* **179**(2), 687–699.

Schwartz M. O. (1997) Mercury in zinc deposits: economic geology of a polluting element. *Int. Geol. Rev.* **39**, 905–992.

Selin N. E. (2009) Global biogeochemical cycling of mercury: a review. *Annu. Rev. Environ. Resour.* **34**, 43–63.

Sherman L. S., Blum J. D., Nordstrom D. K., McCleskey R. B., Barkay T. and Vetriani C. (2009) Mercury isotopic composition of hydrothermal systems in the Yellowstone Plateau volcanic field and Guaymas Basin sea-floor rift. *Earth Planet. Sci. Lett.* **279**(1–2), 86–96.

Smith C. N., Kesler S. E., Klaue B. and Blum J. D. (2005) Mercury isotope fractionation in fossil hydrothermal systems. *Geology* **33**(10), 825–828.

Smith C. N., Kesler S. E., Blum J. D. and Rytuba J. J. (2008) Isotope geochemistry of mercury in source rocks, mineral deposits and spring deposits of the California Coast Ranges, USA. *Earth Planet. Sci. Lett.* **269**(3–4), 399–407.

Smith C. N. (2010) *Isotope Geochemistry of Mercury in Active and Fossil Hydrothermal Systems* PhD Thesis. University of Michigan, Ann Arbor.

Sonke J. E., Schäfer J., Chmeleff J., Audry S., Blanc G. and Dupré B. (2010) Sedimentary mercury stable isotope records of atmospheric and riverine pollution from two major European heavy metal refineries. *Chem. Geol.* **279**(3–4), 90–100.

Spivack A. J. and Edmond J. M. (1987) Boron isotope exchange between seawater and the oceanic crust. *Geochim. Cosmochim. Acta* **51**(5), 1033–1043.

Stoffers P., Hannington M., Wright I., Herzig P. and De Ronde C. (1999) Elemental mercury at submarine hydrothermal vents in the Bay of Plenty, Taupo volcanic zone, New Zealand. *Geology* **27**(10), 931–934.

Štrok M., Baya P. A. and Hintelmann H. (2015) The mercury isotope composition of Arctic coastal seawater. *C.R. Geosci.* **347**(7–8), 368–376.

Sun C., Wu Z., Tao C., Ruan A., Zhang G., Guo Z. and Huang E. (2018) The deep structure of the Duanqiao hydrothermal field at the Southwest Indian Ridge. *Acta Oceanolog. Sin.* **37**(3), 73–79.

Sunderland E. M. and Mason R. P. (2007) Human impacts on open ocean mercury concentrations. *Global Biogeochem. Cycles* **21**(4).

Tao C. H., Lin J., Guo S. Q., John Chen Y. S., Wu G. H., Han X. Q., German C. R., Yoerger D. R., Zhou N., Li H. M., Su X. and Zhu J. (2012) First active hydrothermal vents on an ultraslow-spreading center: Southwest Indian Ridge. *Geology* **40**(1), 47–50.

Tao C., Li H., Jin X., Zhou J., Wu T., He Y., Deng X., Zhang G. and Liu W. (2014) Seafloor hydrothermal activity and polymetallic sulfide exploration on the southwest Indian ridge. *Chin. Sci. Bull.* **59**(19), 2266–2276.

Tao C., Seyfried W. E., Lowell R. P., Liu Y. L., Liang J., Guo Z. K., Ding K., Zhang H. T., Liu J., Qiu L., Egorov I., Liao S. L., Zhao M. H., Zhou J. P., Deng X. M., Li H. M., Wang H. C., Cai W., Zhang G. Y., Zhou H. W., Lin J. and Li W. (2020) Deep high-temperature hydrothermal circulation in a detachment faulting system on the ultra-slow spreading ridge. *Nat. Commun.* **11**, 1300. https://doi.org/10.1038/s41467-020-15062-w.

Tang Y., Bi X., Yin R., Feng X. and Hu R. (2017) Concentrations and isotopic variability of mercury in sulfide minerals from the Jinding Zn-Pb deposit, Southwest China. *Ore Geol. Rev.* **90**, 958–969.

Tivey M. K. (2007) Generation of seafloor hydrothermal vent fluids and associated mineral deposits. *Oceanography* **20**(1), 50–65.

Wang X., Cawood P. A., Zhao H., Zhao L., Grasby S. E., Chen Z. Q. and Zhang L. (2019) Global mercury cycle during the end-Permian mass extinction and subsequent Early Triassic recovery. *Earth Planet. Sci. Lett.* **513**, 144–155.

Xu C., Yin R., Peng J., Hurley J. P., Lepak R. F., Gao J., Feng X., Hu R. and Bi X. (2018) Mercury isotope constraints on the source for sediment-hosted lead-zinc deposits in the Changdu area, southwestern China. *Miner. Deposita* **53**(3), 339–352.

Yang W. F. (2017) *Study of Hydrothermal Mineralization of Duanqiao Hydrothermal Field in Southwest Indian Ridge*. Zhejiang University, Hangzhou, PhD Thesis (In Chinese with English abstract).

Yang W., Tao C., Li H., Liang J., Liao S., Long J., Ma Z. and Wang L. (2017) 230 Th/238 U dating of hydrothermal sulfides from Duanqiao hydrothermal field, Southwest Indian Ridge. *Marine Geophys. Res.* **38**(1–2), 71–83.

Yin R., Feng X., Li Z., Zhang Q., Bi X., Li G., Liu J., Zhu J. and Wang J. (2012) Metallogeny and environmental impact of Hg in Zn deposits in China. *Appl. Geochem.* **27**(1), 151–160.

Yin R., Feng X., Wang J., Li P., Liu J., Zhang Y., Chen J., Zheng L. and Hu T. (2013) Mercury speciation and mercury isotope fractionation during ore roasting process and their implication to source identification of downstream sediment in the Wanshan mercury mining area, SW China. *Chem. Geol.* **336**, 72–79.

Yin R., Feng X., Chen B., Zhang J., Wang W. and Li X. (2015) Identifying the sources and processes of mercury in subtropical estuarine and ocean sediments using Hg isotopic composition. *Environ. Sci. Technol.* **49**(3), 1347–1355.

Yin R., Feng X., Hurley J. P., Krabbenhoft D. P., Lepak R. F., Hu R., Zhang Q., Li Z. and Bi X. (2016a) Mercury isotopes as proxies to identify sources and environmental impacts of mercury in sphalerites. *Sci. Rep.* **6**, 18686. https://doi.org/10.1038/srep18686.

Yin R., Krabbenhoft D. P., Bergquist B. A., Zheng W., Lepak R. F. and Hurley J. P. (2016b) Effects of mercury and thallium concentrations on high precision determination of mercury isotopic composition by Neptune Plus multiple collector inductively coupled plasma mass spectrometry. *J. Anal. At. Spectrom.* **31**(10), 2060–2068.

Yin R., Xu L., Lehmann B., Lepak R. F., Hurley J. P., Mao J., Feng X. and Hu R. (2017) Anomalous mercury enrichment in Early Cambrian black shales of South China: mercury isotopes indicate a seawater source. *Chem. Geol.* **467**, 159–167.

Yin R., Guo Z., Hu L., Liu W., Hurley J. P., Lepak R. F., Feng X. and Li X. (2018) Mercury inputs to Chinese marginal seas: impact of industrialization and development of China. *J. Geophys. Res. Oceans* **123**(8), 5599–5611.

Yin R., Deng C., Lehmann B., Sun G., Lepak R. F., Hurley J. P., Zhao C., Xu G., Tan Q., Xie Z. and Hu R. (2019) Magmatic-hydrothermal origin of mercury in Carlin-style and epithermal gold deposits in China: evidence from mercury stable isotopes. *ACS Earth Space Chem.*. https://doi.org/10.1021/acsearthspacechem.9b00111.

Yue X., Li H., Ren J., Tao C., Zhou J., Wang Y. and Lü X. (2019) Seafloor hydrothermal activity along mid-ocean ridge with strong melt supply: study from segment 27, southwest Indian ridge. *Sci. Rep.* **9**(1), 9874.

Zambardi T., Sonke J. E., Toutain J. P., Sortino F. and Shinohara H. (2009) Mercury emissions and stable isotopic compositions at Vulcano Island (Italy). *Earth Planet. Sci. Lett.* **277**(1–2), 236–243.

Zhang Y., Jacob D. J., Dutkiewicz S., Amos H. M., Long M. S. and Sunderland E. M. (2015) Biogeochemical drivers of the fate of riverine mercury discharged to the global and Arctic oceans. *Global Biogeochem. Cycles* **29**(6), 854–864.

Zheng W. and Hintelmann H. (2010) Nuclear field shift effect in isotope fractionation of mercury during abiotic reduction in the absence of light. *J. Phys. Chem. A* **114**(12), 4238–4245.

Zhu C., Wen H., Zhang Y., Fu S., Fan H. and Cloquet C. (2017) Cadmium isotope fractionation in the Fule Mississippi Valley-type deposit, Southwest China. *Mineralium Deposita* **52**(5), 675–686.

Associate editor: Jun-ichiro Ishibashi